Stability Analysis of DC Microgrid Clusters Based on Step-by-step System Matrix Building Algorithm

K. Jithin, *Graduate Student Member*, *IEEE*, N. Mayadevi, R. Hari Kumar, *Senior Member*, *IEEE*, and V. P. Mini

***Abstract*—DC microgrids (DCMGs) are made up of a network of sources and loads that are connected by a number of power electronic converters (PECs). The increase in the number of these PECs instigates major concerns in system stability. While interconnecting the microgrids to form a cluster, the system stability must be ensured. This paper proposes a novel step-by-step system matrix building (SMB) algorithm to update the system matrix of an existing DCMG cluster when a new microgrid is added to the cluster through a distribution line. The stability of the individual DCMGs and the DCMG cluster is analyzed using the eigenvalue method. Further, the particle swarm optimization (PSO) algorithm is used to retune the controller gains if the newly formed cluster is not stable. The simulation of the DCMG cluster is carried out in MATLAB/Simulink environment to test the proposed algorithm. The results are also validated using the OP4510 real-time simulator (RTS).**

***Index Terms*—Converter, DC microgrid, cluster, eigenvalue, interconnection, particle swarm optimization, system stability, system matrix.**

I. Introduction

DUE to the growing market for DC loads and sources as well as their numerous advantages, DC microgrids (DCMGs) have attained a prominent role nowadays [1], [2]. The power electronic converters (PECs) interface the majority of the sources and loads of a DCMG to a shared DC bus. Therefore, it is possible to characterize power flow, stability, power quality, etc, as a function of converter behavior and their control loops [3], [4].

Various energy storage devices like batteries and flywheels are introduced in the DCMG to tackle the inertia challenges that arise due to the high penetration of renewable energy sources (RESs). However, the capacity limitations and charging and discharging complications raise concerns [5], [6]. As a result, the clustering of grids becomes a more effective and dependable way to get around these problems. The development of clusters of various DCMGs can increase system resilience by diminishing the need for energy storage and enabling seamless power sharing within the grid. However, for clustered DCMGs as autonomous grids, clustered DCMGs are faced with challenges in many aspects including stability, voltage regulation, variable consumer needs, and power quality pose challenges [7]-[9]. Numerous researchers have recently examined DCMG stability problems. One of the widely used techniques for assessing the dynamic stability of the DCMG is small-signal (SS) stability analysis [10]. An investigation of the SS stability of the DCMG cluster based on impedance is performed in [11]. The SS model based on the impedance of the cluster is generated, and the system stability is examined using the eigenvalues. The stability of the low-frequency modes of the DCMG is examined using mesh analysis employing the control method in [12]. A sensitivity analysis is also performed to study how the system parameters affect the stability. A grid-connected DCMG with a hybrid photovoltaic (PV) and wind is assessed for its stability in [13]. Reference [14] discusses several restrictions connected to the traditional stability criteria such as right-half-plane (RHP) poles or subsystem zeros. Additionally, impedance-based criteria for stability are proposed for multi-bus DCMGs in the light of generalized Bode plots.

Using eigenvalue observation, a state space model of the DCMG is created in [15] to examine the effects of the suggested optimized secondary controller on DCMG stability. The admittance matrix is generated and factorized using a separate methodology and the attainment of stability requirements for droop-controlled DCMGs with different loads is facilitated and ensured by the admittance matrix modification technique in [16]. The design and stability study of a DCMG with a hybrid energy storage system with operating voltages of different supercapacitor is covered in [17]. Reference [18] discusses large-signal stability of DCMG using a system-level method. Reference [19] suggests a Takagi-Sugeno multi-modeling method based large-signal stability study of DCMG clusters. The analysis is simplified by reducing the large-signal Lyapunov stability of DCMG cluster to the computation of a number of linear matrix inequalities. Using

Manuscript received: February 1, 2023; revised: April 3, 2023; accepted: July 6, 2023. Date of CrossCheck: July 6, 2023. Date of online publication: August 8, 2023.

K. Jithin (corresponding author), N. Mayadevi, R. H. Kumar, and V. P. Mini are with the Department of Electrical Engineering, College of Engineering Trivandrum, APJ Abdul Kalam Technological University (APJAKTU), Thiruvananthapuram, India (e-mail: d-tve19jan029@cet. ac. in; maya@cet. ac. in; harikumar@cet.ac.in; minivp@cet.ac.in).

DOI: 10.35833/MPCE.2023.000054

a boost converter and a bidirectional DC-DC converter with the Lyapunov function, the DCMG stability is investigated in [20]. The relationship between system parameters and stability is presented and discussed in [21].

The stability criterion evaluates and guarantees the system stability under significant disturbance in the design phase rather than repeatedly computing and simulating. In [22], various stability analysis and control techniques with interconnected MGs are studied and compared. The MG is described as a medium- and high-dimensional negative feedback loop in [23]. Also, a stability criterion based on the extended Gershgorin theorem with a wide eigenvalue range is developed. In [24], stability analysis considering constant delay and time-varying delay utilizing linear matrix inequality is performed. In order to satisfy the requirements for power balance and grid voltage stability, the non-linear MG model is introduced, and a thorough stability study is performed in [25].

Reference [26] proposes a partitioning strategy with stability constraints based on SS stability. Moreover, a novel index for the marginal stability of the MG is defined using sensitivity analysis of droop gain. A buck converter-based DCMG is developed in [27] and its robustness and stability are assessed using the Kharitonov theorem and root locus, respectively. It is proven that an increase in constant power loads causes a decrease in system stability.

Even though, various techniques are available for the stability analysis of DCMG, and the effect of the interconnection of MGs to form a cluster on stability is not considered yet. This paper examines the stability of a DCMG cluster using an eigenvalue-based method. A step-by-step system matrix building (SMB) algorithm that avoids the need to completely rebuild a system matrix of cluster whenever a new DCMG is interconnected to it when a distribution line is developed and analyzed. To ensure the reliable functioning of the cluster, the optimization of controller gains utilizing particle swarm optimization (PSO) is also carried out. Through time response analysis, simulation, and real-time experimentation, the proposed algorithm has been validated.

The rest of the paper is structured as follows. Section II presents the transfer function of converter-based DCMGs. The stability analysis of individual DCMG is presented in Section III. The development of the system matrix of a clustered network from the system matrix of the individual networks, when interconnected through a distribution line, is presented in Section IV. Section V presents the stability analysis of the DCMG clusters. Section VI presents the simulation results. Section VII presents a real-time analysis of the DCMG cluster and Section VIII concludes this paper.

II. Transfer Function of Converter-based DCMGs

A DCMG consists of distributed energy resources (DERs), loads, converters, and controllers. All the sources and loads in a DCMG are interfaced with the main bus using DC-DC converters and hence they have a significant role in the stable and reliable operation of the MG. The transfer function of DCMG is developed using the SS model.

The transfer functions are shown in Table I, where $D' = 1 - D$ and $den(s) = s^2LCR + sL + RD'^2$, and D is the duty cycle. The duty cycle to the output voltage and duty cycle to inductor current transfer functions G_{vd} and G_{id} of the converters are listed in Table I [28], where L and C are the converter reactive elements; V_{in} is the input to the converter; V_o is the output of the converter; and R is the load in the system. The simplified representations of DCMGs with non-dispatchable and dispatchable sources are given in Figs. 1 and 2, respectively, where V_{bus} is the bus voltage; I_{Ln} is the inductor current; and d is the duty ratio. PWM stands for paulse width modulation. For systems with non-dispatchable sources, the reference input to the controller is V_{ref}, and for systems with dispatchable sources, it is I_{ref}.

TABLE I
Transfer Functions of Converters

Converter	G_{vd}	G_{id}
Buck	$RV_{in}/(s^2LCR + sL + R)$	$(1 + sCR)V_{in}/(s^2LCR + sL + R)$
Boost	$(RD'^2 - sL)V_{in}/den(s)D'^2$	$(2 + sCR)V_{in}/den(s)D'$

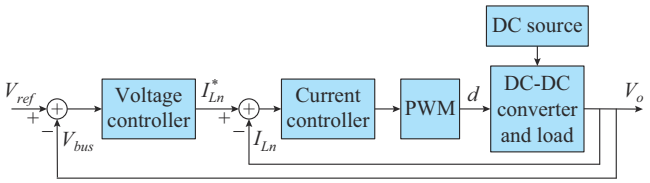

Fig. 1. Block diagram of DCMG with non-dispatchable sources.

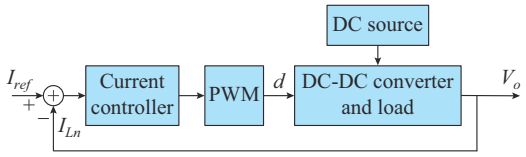

Fig. 2. Block diagram of DCMG with dispatchable sources.

The central controller, which employs an algorithm for the optimal dispatch, provides the value of I_{ref} [29]. The controller gains are obtained using Ziegler-Nichols method [30], [31].

A. Solar PV System with Boost Converter

The solar PV system with boost converter can be represented by the block diagram as shown in Fig. 3, where V_{pv} is the output voltage of PV; $V_{ref,pv}(s)$ is the reference voltage of PV; $I_{L,pv}(s)$ is the inductor current of PV converter; and $V_{o,pv}(s)$ is the output voltage of PV converter. The overall transfer function of the system is derived by reducing the control loops and substituting the parameter values from Table II.

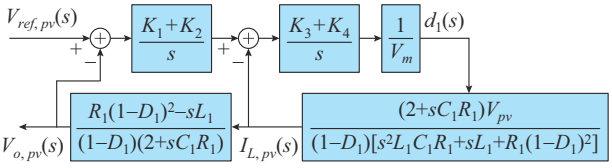

Fig. 3. Block diagram of solar PV system with boost converter.

The values of these gains are obtained by tuning.

TABLE II
DESIGN PARAMETERS FOR SOLAR PV SYSTEM AND WIND GENERATION SYSTEM

Parameter	Solar PV system	Wind generation system
Converter inductance	$L_1=45$ mH	$L_2=45$ mH
Converter capacitance	$C_1=25$ mF	$C_2=5$ mF
Load	$R_1=30\ \Omega$	$R_2=27\ \Omega$
Output voltage	$V_{pv}=80$ V	$V_W=300$ V
Proportional gain of voltage controller	$K_1=0.09$	$K_5=0.1$
Integral gain of voltage controller	$K_2=1$	$K_6=0.55$
Proportional gain of current controller	$K_3=0.1$	$K_7=0.1$
Integral gain of current controller	$K_4=5$	$K_8=0.1$
PWM gain	$V_m=4$	$V_m=4$
Duty cycle	$D_1=0.22$	$D_2=0.33$

The overall transfer function of solar PV system with boost converter $V_{o,pv}(s)/V_{ref,pv}(s)$ is obtained as (1).

$$\frac{V_{o,pv}(s)}{V_{ref,pv}(s)}=\frac{-0.0024\times10^{-4}s^4+0.82s^3+109s^2+2796s+96000}{0.00065s^5+0.06s^4+8.72s^3+332s^2+4256s+19200} \tag{1}$$

B. Wind Generation System with Buck Converter

The block diagram of a wind generation system with buck converter is shown in Fig. 4, where the subscript *WG* denotes the wind generation.

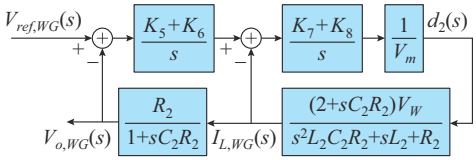

Fig. 4. Block diagram of a wind generation system with buck converter.

Rectifier dynamics are neglected in this paper. The values of the gains (K_5-K_8) are obtained by tuning the controllers. The overall transfer function of the wind generation system $V_{o,WG}(s)/V_{ref,WG}(s)$ is derived by reducing the block diagram and substituting the parameter values from Table II and is obtained as (2).

$$\frac{V_{o,WG}(s)}{V_{ref,WG}(s)}=\frac{10.93s^3+152.07s^2+586.64s+446}{0.0033s^5+0.06s^4+34.3s^3+298s^2+204s+445.5} \tag{2}$$

C. Fuel Cell with Boost Converter

Block diagram of a fuel cell with the boost converter is shown in Fig. 5, where the subscript *FC* denotes the fuel cell.

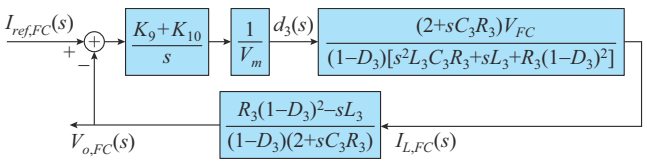

Fig. 5. Block of a fuel cell with boost converter.

The overall transfer function of the system, derived by reducing the block diagram in Fig. 5 and substituting the parameter values from Table III, is obtained as (3). The values of the proportional and integral gains of the current controller, K_9 and K_{10}, respectively, are obtained by tuning the controller.

$$\frac{V_{o,FC}(s)}{I_{ref,FC}(s)}=\frac{-0.00275s^2+1.114s+332.8}{0.00025s^3+0.029s^2+8.8s+121} \tag{3}$$

TABLE III
DESIGN PARAMETERS FOR FUEL CELL AND BATTERY SYSTEM

Parameter	Fuel cell	Battery system
Converter inductance	$L_3=0.5$ mH	$L_4=1$ mH
Converter capacitance	$C_3=7.5$ mF	$C_4=1$ mF
Load	$R_3=10\ \Omega$	$R_4=10\ \Omega$
Output voltage	$V_{FC}=55$ V	$V_{bat}=48$ V
Proportional gain of current controller	$K_9=0.01$	$K_{11}=K_{12}=0.01$
Integral gain of current controller	$K_{10}=2$	$K_{13}=K_{14}=8$
PWM gain	$v_m=4$	$v_m=4$
Duty cycle	$D_3=0.45$	$D_4=0.6$

D. Battery Energy Storage System (BESS) with Bidirectional Converter

The BESS works in either a buck or boost mode based on the charging/discharging operation. For deriving the transfer function, each mode is considered separately.

1) BESS Operating in Buck Mode

Figure 6 shows the block diagram of BESS operating in buck mode, where the subscript *B*1 denotes the BESS in buck mode. K_{11} and K_{12} are the proportional and integral gains of the current controller. The overall transfer function of BESS with converter operating in buck mode, after substituting the values from Table III, is obtained as (4).

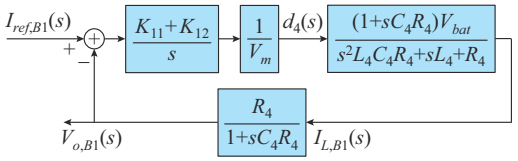

Fig. 6. Block diagram of BESS operating in buck mode.

$$\frac{V_{o,B1}(s)}{I_{ref,B1}(s)}=\frac{4.8s+3840}{0.00004s^3+0.048s^2+50.3s+384} \tag{4}$$

2) BESS Operating in Boost Mode

Figure 7 shows the block diagram of BESS operating in boost mode, where the subscript *B*2 denotes the BESS in boost mode. The overall transfer function of the BESS operating in boost mode, after substituting the parameter values from Table III, is obtained as (5).

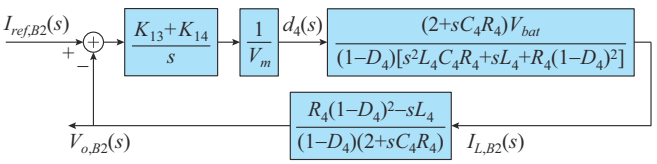

Fig. 7. Block diagram of BESS operating in boost mode.

$$\frac{V_{o,B2}(s)}{I_{ref,B2}(s)} = \frac{-0.00048s^2 + 0.384s + 614.4}{0.0000025s^3 + 0.0027s^2 + 2.9s + 307.2} \quad (5)$$

III. Stability Analysis of Individual DCMGs

The stability analysis of individual DCMGs is carried out by computing the eigenvalues using the state space model obtained from the transfer function of sources.

A. MG1

The transfer function of the solar PV system in (1) is used to model MG1. The transfer function is converted to the state space model and the system matrix $\boldsymbol{A}_{MG1}$ of MG1 is obtained as (6).

$$\boldsymbol{A}_{MG1} = \begin{bmatrix} -91.81 & -105.1 & -62.53 & -25.05 & -14.13 \\ 128 & 0 & 0 & 0 & 0 \\ 0 & 64 & 0 & 0 & 0 \\ 0 & 0 & 32 & 0 & 0 \\ 0 & 0 & 0 & 8 & 0 \end{bmatrix} \quad (6)$$

B. MG2

The transfer function of the wind generation system in (2) is used to model MG2, and the system matrix $\boldsymbol{A}_{MG2}$ is obtained as (7).

$$\boldsymbol{A}_{MG2} = \begin{bmatrix} -181.5 & -81.78 & -22.19 & -3.798 & -2.072 \\ 128 & 0 & 0 & 0 & 0 \\ 0 & 32 & 0 & 0 & 0 \\ 0 & 0 & 4 & 0 & 0 \\ 0 & 0 & 0 & 4 & 0 \end{bmatrix} \quad (7)$$

C. MG3

The system matrix of MG3 $\boldsymbol{A}_{MG3}$ is obtained using the transfer function of the fuel cell in (3) and is given in (8).

$$\boldsymbol{A}_{MG3} = \begin{bmatrix} -115.2 & -137.8 & -59.19 \\ 256 & 0 & 0 \\ 0 & 32 & 0 \end{bmatrix} \quad (8)$$

D. MG4

In this analysis, the BESS operating in boost mode is considered. The transfer function in (5) is used for the model and the system matrix is obtained as (9).

$$\boldsymbol{A}_{MG4} = \begin{bmatrix} -1000 & -1123 & -457.8 \\ 1024 & 0 & 0 \\ 0 & 256 & 0 \end{bmatrix} \quad (9)$$

The eigenvalues of individual DCMGs shown in Fig. 8 is generated using the system matrices of the individual DCMGs. As long as the systems are stable, all their eigenvalues are located in the left half of the *s*-plane.

IV. System Matrix of a Clustered Network: Theoretical Evaluation

To analyze the impact of interconnection during the formation of clusters, the RLC network shown in Fig. 9 with V_1 as input and V_2 as output is considered.

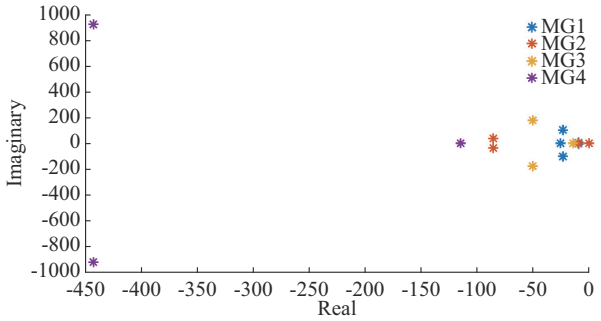

Fig. 8. Eigenvalues of individual DCMGs.

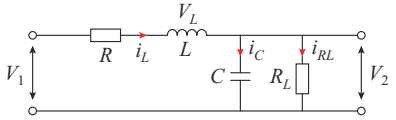

Fig. 9. RLC network.

V_L is the voltage across inductor; i_C is the current through capacitor; i_{RL} is the current through the load; R_L is the load resistance; and i_L is the state variable.

The state space model is given in (10). In this paper, three cases analyzed are ① adding a new network to an existing network via a distribution line, ② adding a new network in between a distribution line, and ③ adding a new network at one end of a distribution in a cluster.

$$\begin{bmatrix} \frac{di_L}{dt} \\ \frac{dV_c}{dt} \end{bmatrix} = \begin{bmatrix} \frac{-R}{L} & \frac{-1}{L} \\ \frac{1}{C} & \frac{-1}{R_L C} \end{bmatrix} \begin{bmatrix} i_L \\ V_c \end{bmatrix} + \begin{bmatrix} \frac{1}{L} \\ 0 \end{bmatrix} V_1 \quad (10)$$

where V_c is the voltage across capacitor.

A. Case 1: Adding a New Network to an Existing Network

This subsection analyses the modifications that need to be made to the system matrix when a new network is interconnected through the distribution line to an existing network. Figure 10 shows new RLC network added to an existing network through a distribution line. R_{TL} and L_{TL} are the resistance and the inductance of the distribution line, respectively; V_{R1} and V_{R2} are the voltages across the line resistances R_1 and R_2, respectively; and i_{LTL} is the current through the distribution line.

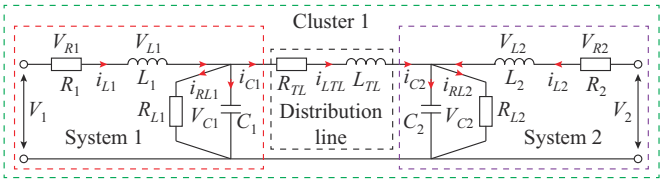

Fig. 10. New RLC network added to an existing network through a distribution line.

The system matrix of the interconnected network is represented by (11).

$$\boldsymbol{A}_{C1}=\overbrace{\begin{bmatrix}\frac{-R_1}{L_1} & \frac{-1}{L_1} & 0 & 0 & 0\\ \frac{1}{C_1} & \frac{-1}{R_{L1}C_1} & \frac{-1}{C_1} & 0 & 0\\ 0 & \frac{1}{L_{TL}} & \frac{-R_{TL}}{L_{TL}} & 0 & \frac{-1}{L_{TL}}\\ 0 & 0 & 0 & \frac{-R_2}{L_2} & \frac{-1}{L_2}\\ 0 & 0 & \frac{1}{C_2} & \frac{1}{C_2} & \frac{-1}{R_{L2}C_2}\end{bmatrix}}^{\text{System 1}}_{\text{System 2}} \tag{11}$$

It can be observed from a comparison of the system matrices in (10) and (11) that the system matrices of the individual networks are added diagonally. In addition, an additional row and column are introduced to accommodate the coupling due to the distribution line.

The value of the diagonal element corresponding to the additional row and column is equal to the negative of the resistance to inductance ratio of the distribution line. The magnitude of the off-diagonal elements is equal to the inverse of the inductance and capacitance of the distribution line at both ends. The paper reveals that it is possible to create a step-by-step algorithm for updating the system matrix.

Consider the graphical representation of the interconnected networks shown in Fig. 11. We can let: ① $\boldsymbol{A}_C$ be the system matrix of the single network with dimension of $m\times m$; ② $\boldsymbol{A}_S$ be the system matrix of the incoming network with dimension of $n\times n$; ③ i^{th} row of $\boldsymbol{A}_C$ correspond to the state equation of the state variable associated with the capacitor C_i connected to node i; and ④ j^{th} row of $\boldsymbol{A}_S$ correspond to the state equation of the state variable associated with the capacitor C_j connected to node j.

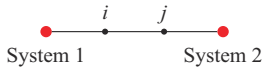

Fig. 11. Graphical representation of adding a new network to an existing network.

The system matrix can be updated as follows.

1) Create matrix $\boldsymbol{A}_{U1}$ by adding one row and one column to the system matrix $\boldsymbol{A}_C$ to accommodate the elements corresponding to the distribution line.

2) Obtain $\boldsymbol{A}_{C1}$ by adding $\boldsymbol{A}_S$ to the system matrix $\boldsymbol{A}_{U1}$ diagonally.

3) Update the elements corresponding to the distribution line in $\boldsymbol{A}_{C1}$ as follows: $A_{C1}(m+1,m+1)=-R_{TL}/L_{TL}$; $A_{C1}(i,m+1)=-1/C_i$; $A_{C1}(m+1+j,m+1)=1/C_j$; $A_{C1}(m+1,i)=1/L_{TL}$; and $A_{C1}(m+1,m+1+j)=-1/L_{TL}$.

The system matrix of the interconnected system will be a $(m+1+n)\times(m+1+n)$ matrix and is given by (12).

$$\boldsymbol{A}_{C1}=\overbrace{\begin{bmatrix}a_{11} & a_{12} & \cdots & a_{1i} & \cdots & a_{1m} & 0 & 0 & \cdots & 0 & \cdots & 0\\ a_{21} & a_{22} & \cdots & a_{2i} & \cdots & a_{2m} & 0 & 0 & \cdots & 0 & \cdots & 0\\ \vdots & \vdots & & \vdots & & \vdots & \vdots & \vdots & & \vdots & & \vdots\\ a_{i1} & a_{i2} & \cdots & a_{ii} & \cdots & a_{im} & -\frac{1}{C_i} & 0 & \cdots & 0 & \cdots & 0\\ \vdots & \vdots & & \vdots & & \vdots & \vdots & \vdots & & \vdots & & \vdots\\ a_{m1} & a_{m2} & \cdots & a_{mi} & \cdots & a_{mm} & 0 & 0 & \cdots & 0 & \cdots & 0\\ 0 & 0 & \cdots & \frac{1}{L_{TL}} & \cdots & 0 & -\frac{R_{TL}}{L_{TL}} & 0 & \cdots & -\frac{1}{L_{TL}} & \cdots & 0\\ 0 & 0 & \cdots & 0 & \cdots & 0 & 0 & a_{(m+2)(m+2)} & \cdots & a_{(m+2)j} & \cdots & a_{(m+2)(m+1+n)}\\ \vdots & \vdots & & \vdots & & \vdots & \vdots & \vdots & & \vdots & & \vdots\\ 0 & 0 & \cdots & 0 & \cdots & 0 & -\frac{1}{C_j} & a_{(m+1+j)(m+2)} & \cdots & a_{(m+1+j)j} & \cdots & a_{(m+1+j)(m+1+n)}\\ \vdots & \vdots & & \vdots & & \vdots & \vdots & \vdots & & \vdots & & \vdots\\ 0 & 0 & \cdots & 0 & \cdots & 0 & 0 & a_{(m+1+n)(m+2)} & \cdots & a_{(m+1+n)j} & \cdots & a_{(m+1+n)(m+1+n)}\end{bmatrix}}^{\text{System 1}}_{\text{System 2}} \tag{12}$$

The proposed algorithm has the advantage that, the addition of a new system to the existing cluster does not require a complete rebuilding of the system matrix.

B. Case 2: Adding a New Network in Between a Distribution Line

Figure 12 shows a new RLC network in between the distribution line, which has system 1 and system 2 connected via a distribution line T_L and system 3 connected through a distribution line T_{L3} in between the former distribution line. V_0 is the voltage assumed at the point of interconnection. The system matrix of the complete network is given by (13). The current cluster consists of two systems, system 1 and system 2, which are coupled by a distribution line running between nodes i and j. The incoming network, system 3, is connected to a point (node p) on the distribution line that links nodes i and j through a distribution line as shown in Fig. 13. It is assumed that the current of new distribution line flows from node l to node p.

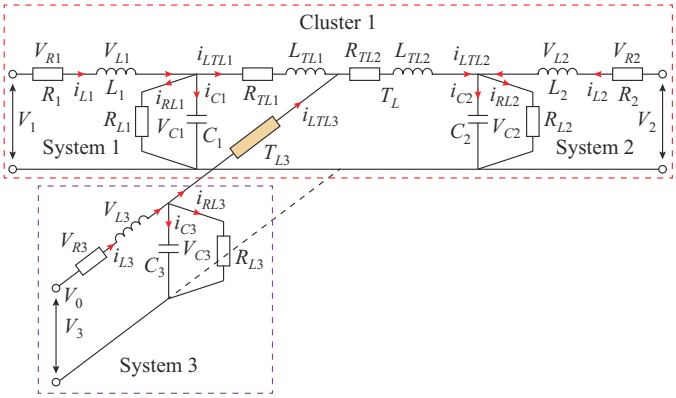

Fig. 12. A new network in between a distribution line.

$$A_{C2}=\begin{bmatrix}
\frac{-R_1}{L_1} & \frac{-1}{L_1} & 0 & 0 & 0 & 0 & 0 & 0 & 0\\
\frac{1}{C_1} & \frac{-1}{R_{L1}C_1} & \frac{-1}{C_1} & 0 & 0 & 0 & 0 & 0 & 0\\
0 & \frac{1}{L_{TL1}} & \frac{-R_{TL1}}{L_{TL1}} & 0 & 0 & 0 & 0 & 0 & 0\\
0 & 0 & 0 & \frac{-R_2}{L_2} & \frac{-1}{L_2} & 0 & 0 & 0 & 0\\
0 & 0 & 0 & \frac{1}{C_2} & \frac{-1}{R_{L2}C_2} & \frac{-1}{C_2} & 0 & 0 & 0\\
0 & 0 & 0 & 0 & \frac{1}{L_{TL2}} & \frac{-R_{TL2}}{L_{TL2}} & 0 & 0 & 0\\
0 & 0 & 0 & 0 & 0 & 0 & \frac{-R_{TL3}}{L_{TL3}} & 0 & \frac{1}{L_{TL3}}\\
0 & 0 & 0 & 0 & 0 & 0 & 0 & \frac{-R_3}{L_3} & \frac{-1}{L_3}\\
0 & 0 & 0 & 0 & 0 & 0 & \frac{-1}{C_3} & \frac{1}{C_3} & \frac{-1}{R_{L3}C_3}
\end{bmatrix}$$

(13)

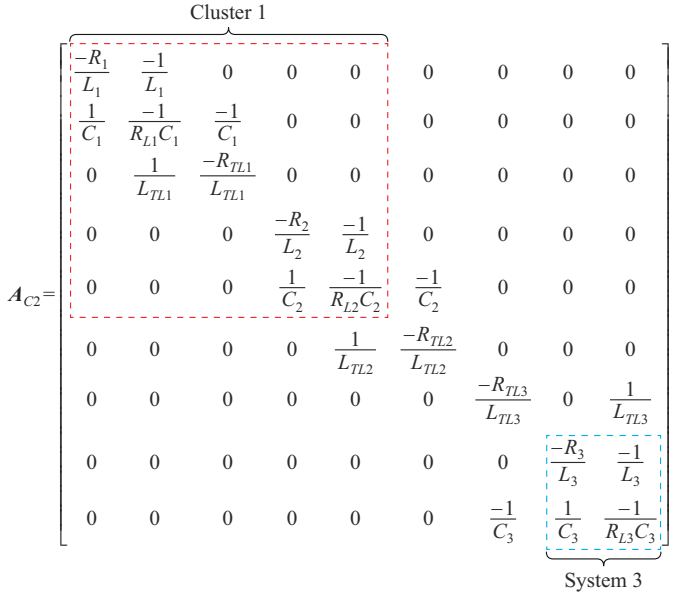

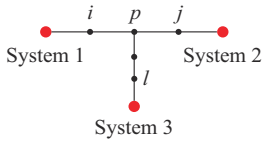

Fig. 13. Graphical representation of adding a new network in between a distribution line.

We can let: ① $\boldsymbol{A}_C$ be the system matrix of cluster with dimension of $m \times m$; ② $\boldsymbol{A}_S$ be the system matrix of the incoming network with dimension of $n \times n$; ③ i^{th} row of $\boldsymbol{A}_C$ correspond to the state equation of the state variable associated with the capacitor C_i connected to node i; ④ j^{th} row of $\boldsymbol{A}_C$ correspond to the state equation of the state variable associated with the capacitor C_j connected to node j; ⑤ k^{th} row of $\boldsymbol{A}_C$ correspond to the state equation of the state variable associated with the inductance of line between node i and node j; and ⑥ first row of $\boldsymbol{A}_S$ correspond to the state equation of the state variable associated with the capacitor C connected to node l.

The existing distribution line with resistance R_{TL} and inductance L_{TL} is split into two sections: ① the first section has resistance $R_{TL1}=aR_{TL}$ and inductance $L_{TL1}=aL_{TL}$; and ② the second section has resistance $R_{TL2}=bR_{TL}$ and inductance $L_{TL2}=bL_{TL}$, where $a+b=1$. The system matrix of the original cluster must be augmented with an additional row and column in order to account for this splitting. The system matrix of the interconnected system can be obtained as follows.

1) Create matrix $\boldsymbol{A}_{U1}$ by adding one row and one column to the system matrix $\boldsymbol{A}_C$ to accommodate the elements corresponding to the distribution line that is split into two sections due to interconnection.

2) Create matrix $\boldsymbol{A}_{U2}$ by adding one row and one column to the system matrix $\boldsymbol{A}_C$ to accommodate the elements corresponding to the new distribution line with R_{TL3} and L_{TL3}.

3) Obtain $\boldsymbol{A}_{C2}$ by adding $\boldsymbol{A}_S$ to the system matrix $\boldsymbol{A}_{U2}$ diagonally.

4) Update the values corresponding to the distribution line in $\boldsymbol{A}_{C2}$ as follows: $A_{C2}(k,k)=-R_{TL1}/L_{TL1}=-aR_{TL}/(aL_{TL})=-R_{TL}/L_{TL}$; $A_{C2}(k,i)=1/L_{TL1}=1/(aL_{TL})$; $A_{C2}(k,j)=0$; $A_{C2}(j,k)=0$; $A_{C2}(m+1,m+1)=-R_{TL2}/L_{TL2}=-bR_{TL}/(bL_{TL})=-R_{TL}/L_{TL}$; $A_{C2}(j,m+1)=-1/C_2$; $A_{C2}(m+1,j)=-1/L_{TL2}=-L_{TL}/b$; $A_{C2}(m+2,m+2)=-R_{TL3}/L_{TL3}$; $A_{C2}(m+2,m+2+l)=-1/L_{TL3}$; and $A_{C2}(m+2+l,m+2)=-1/C_l$.

The dimension of the system matrix of interconnected system $\boldsymbol{A}_{C2}$ will be $(m+2+n)(m+2+n)$.

C. Case 3: Adding a New Network at One End of a Distribution Line in a Cluster

The new network interconnected to one end of a distribution line in a cluster is shown in Fig. 14.

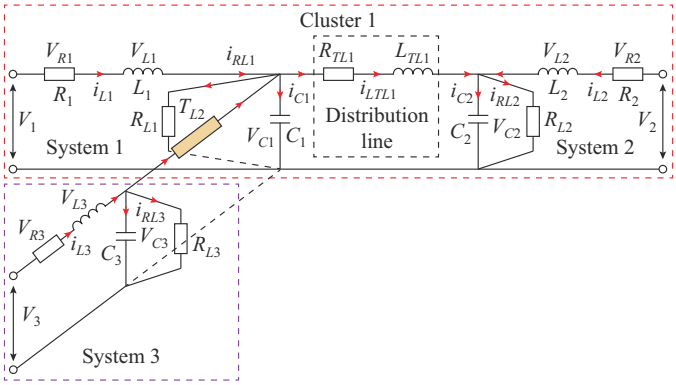

Fig. 14. New network interconnected to one end of a distribution line in a cluster.

A graphical representation of this interconnected network in Fig. 15 is used to create a step-by-step procedure for updating the system matrix whenever a new network is interconnected with an existing network at one end of a distribution line linking two networks in the cluster.

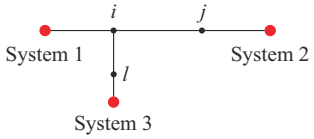

Fig. 15. Graphical representation of adding a new network at one end of distribution line.

The new network is added to the cluster formed in the first case and the assumptions are also the same as in the

previous case. The system matrix can be updated as:

$$
\boldsymbol{A}_{C3}=\left[\begin{array}{cccccccc}
\frac{-R_1}{L_1} & \frac{-1}{L_1} & 0 & 0 & 0 & 0 & 0 & 0 \\
\frac{1}{C_1} & \frac{-1}{R_{L1}C_1} & \frac{-1}{C_1} & 0 & 0 & \frac{1}{C_1} & 0 & 0 \\
0 & \frac{1}{L_{TL1}} & \frac{-R_{TL1}}{L_{TL1}} & 0 & \frac{-1}{L_{TL1}} & 0 & 0 & 0 \\
0 & 0 & 0 & \frac{-R_2}{L_2} & \frac{-1}{L_2} & 0 & 0 & 0 \\
0 & 0 & \frac{1}{C_2} & \frac{1}{C_2} & \frac{-1}{R_{L2}C_2} & 0 & 0 & 0 \\
0 & \frac{-1}{L_{TL2}} & 0 & 0 & 0 & \frac{-R_{TL2}}{L_{TL2}} & 0 & \frac{1}{L_{TL2}} \\
0 & 0 & 0 & 0 & 0 & 0 & \frac{-R_3}{L_3} & \frac{-1}{L_3} \\
0 & 0 & 0 & 0 & 0 & \frac{-1}{C_3} & \frac{1}{C_3} & \frac{-1}{R_{L3}C_3}
\end{array}\right] \tag{14}
$$

(Cluster 1: rows/columns 1–5; System 3: rows/columns 7–8)

1) Create matrix $\boldsymbol{A}_{U1}$ by adding one row and one column to the system matrix $\boldsymbol{A}_C$ to accommodate the elements corresponding to the distribution line with R_{TL2} and L_{TL2}.

2) Obtain $\boldsymbol{A}_{C3}$ by adding $\boldsymbol{A}_S$ to the system matrix $\boldsymbol{A}_{U1}$ diagonally.

3) Update the values corresponding to the distribution line in $\boldsymbol{A}_{C3}$ as follows: $A_{C3}(m+1,m+1)=-R_{TL1}/L_{TL1}$; $A_{C3}(m+1,i)=-1/L_{TL1}$; $A_{C3}(m+1,l)=1/L_{TL1}$; $A_{C3}(i,m+1)=1/C_i$; and $A_{C3}(l,m+1)=-1/C_l$.

The dimension of $\boldsymbol{A}_{C3}$ will be $(m+1+n)(m+1+n)$. The aforementioned analysis shows that, rather than rebuilding the entire system matrix, the system matrix of a cluster, when a new network is interconnected through a distribution line, can be obtained by updating the system matrix of the existing cluster through a simple and direct step-by-step procedure. This method can be applied to develop the system matrix of interconnected DCMGs in order to assess its stability:

$$
\boldsymbol{A}_{C2}=\left[\begin{array}{ccccccccccccccccc}
a_{11} & a_{12} & \cdots & a_{1i} & \cdots & a_{1j} & \cdots & a_{1k} & \cdots & a_{1m} & 0 & 0 & 0 & \cdots & 0 & \cdots & 0 \\
a_{21} & a_{22} & \cdots & a_{2i} & \cdots & a_{2j} & \cdots & a_{2k} & \cdots & a_{2m} & 0 & 0 & 0 & \cdots & 0 & \cdots & 0 \\
\vdots & \vdots & & \vdots & & \vdots & & \vdots & & \vdots & \vdots & \vdots & \vdots & & \vdots & & \vdots \\
a_{i1} & a_{i2} & \cdots & a_{ii} & \cdots & a_{ik} & \cdots & a_{ij} & \cdots & a_{im} & 0 & 0 & 0 & \cdots & 0 & \cdots & 0 \\
\vdots & \vdots & & \vdots & & \vdots & & \vdots & & \vdots & \vdots & \vdots & \vdots & & \vdots & & \vdots \\
0 & 0 & \cdots & \frac{1}{a}\times a_{ki} & \cdots & a_{kk} & \cdots & 0 & \cdots & 0 & 0 & 0 & 0 & \cdots & 0 & \cdots & 0 \\
\vdots & \vdots & & \vdots & & \vdots & & \vdots & & \vdots & \vdots & \vdots & \vdots & & \vdots & & \vdots \\
a_{j1} & a_{j2} & \cdots & a_{ji} & \cdots & 0 & \cdots & a_{jj} & \cdots & a_{jm} & \frac{-1}{C_i} & 0 & 0 & \cdots & 0 & \cdots & 0 \\
\vdots & \vdots & & \vdots & & \vdots & & \vdots & & \vdots & \vdots & \vdots & \vdots & & \vdots & & \vdots \\
a_{m1} & a_{m2} & \cdots & a_{mi} & \cdots & a_{mk} & \cdots & a_{mj} & \cdots & a_{mm} & 0 & 0 & 0 & \cdots & 0 & \cdots & 0 \\
0 & 0 & \cdots & 0 & \cdots & 0 & \cdots & \frac{1}{bL_{TL}} & \cdots & 0 & \frac{-R_{TL}}{L_{TL}} & 0 & 0 & \cdots & 0 & \cdots & 0 \\
0 & 0 & \cdots & 0 & \cdots & 0 & \cdots & 0 & \cdots & 0 & 0 & \frac{-R_{TL3}}{L_{TL3}} & 0 & \cdots & \frac{-1}{L_{TL3}} & \cdots & 0 \\
0 & 0 & \cdots & 0 & \cdots & 0 & \cdots & 0 & \cdots & 0 & 0 & 0 & a_{(m+3)(m+3)} & \cdots & a_{(m+3)l} & \cdots & a_{(m+3)(m+2+n)} \\
\vdots & \vdots & & \vdots & & \vdots & & \vdots & & \vdots & \vdots & \vdots & \vdots & & \vdots & & \vdots \\
0 & 0 & \cdots & 0 & \cdots & 0 & \cdots & 0 & \cdots & 0 & 0 & \frac{-1}{C_1} & a_{(m+2+l)(m+3)} & \cdots & a_{(m+2+l)l} & \cdots & a_{(m+2+l)(m+2+n)} \\
\vdots & \vdots & & \vdots & & \vdots & & \vdots & & \vdots & \vdots & \vdots & \vdots & & \vdots & & \vdots \\
0 & 0 & \cdots & 0 & \cdots & 0 & \cdots & 0 & \cdots & 0 & 0 & 0 & a_{(m+2+n)(m+3)} & \cdots & a_{(m+2+n)l} & \cdots & a_{(m+2+n)(m+2+n)}
\end{array}\right] \tag{15}
$$

(Cluster 1: upper-left block a_{11} to a_{mm}; System 3: lower-right block $a_{(m+3)(m+3)}$ to $a_{(m+2+n)(m+2+n)}$)

V. Stability Analysis of DCMG Clusters

By interconnecting DCMGs to form a DCMG cluster as shown in Fig. 16, the reliability can be enhanced as it overcomes the issues due to storage and intermittent behavior of RESs. However, the stability of DCMGs with high penetration of converter interfaced sources and loads might be a big hurdle, particularly when interconnecting with the existing DCMG clusters. Therefore, it is crucial to investigate how the interconnection affects system stability.

The proposed SMB algorithm developed in Section IV is used to developing the system matrix of the DCMG cluster. Three different scenarios considered are: ① interconnecting two DCMGs through a distribution line; ② adding a DCMG between two buses in a distribution line; and ③ adding a new DCMG at one end of a distribution line in the DCMG cluster.

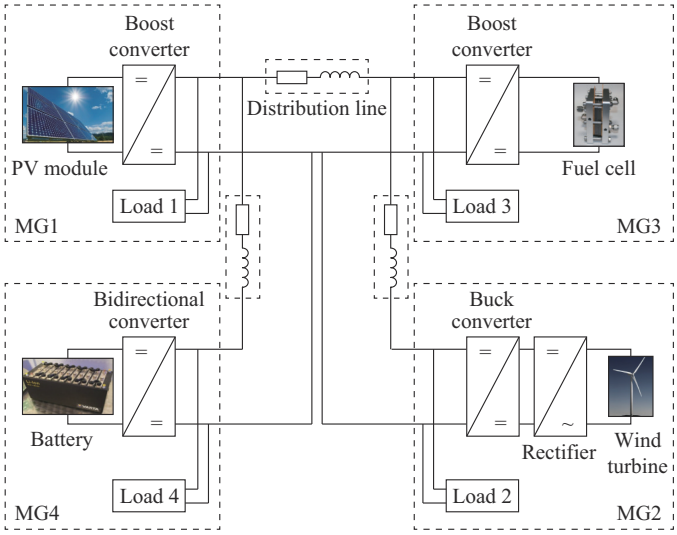

Fig. 16. DCMG cluster.

A. Scenario 1: Formation of a DCMG Cluster Interconnecting Two MGs Using a Distribution Line

A DCMG cluster interconnecting two MGs with a distribution line is shown in Fig. 17, one with a wind generation system as a source and the other with a BESS connected using a distribution line with 0.2 Ω resistance and 50 μH inductance [19]. During the stability analysis, the reliability of the system and dynamic thermal rating (DTR) of the system that determines the optimum rating of power components based on thermal limit can be considered to obtain much more accurate results.

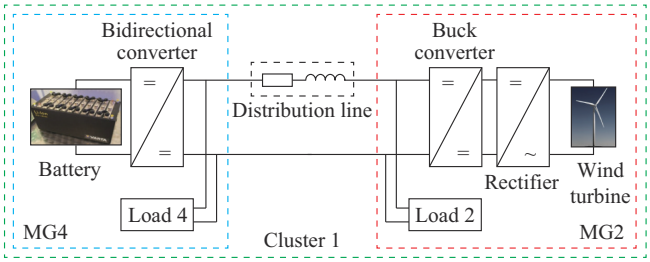

Fig. 17. DCMG cluster interconnecting two MGs with a distribution line.

Rather than choosing random values for cables or overhead lines with some static ratings, the selection of parameters can be done by considering the DTR. Standards like IEEE 738 describe how parameters for overhead lines are selected based on DTR. In this paper, the static rating of the cable is considered for the analysis [32], [33].

In order to improve the precision of a DCMG analysis, all system uncertainties need to be taken into account. Climate, temperature, etc., are very significant when analyzing RESs integrating MG, as intermittent sources like wind and PV are often used in these systems [34]-[36]. These dynamic factors are neglected as the analysis is performed from the perspective of control system.

The system matrix of the DCMG cluster, using the system matrix of the MG2 given in (7) and the system matrix of the MG4 in (9), is obtained using the algorithm developed in Section IV-A and is given in (16).

$$\begin{array}{c} \overbrace{}^{\text{MG1}} \\ \left[\begin{array}{ccccc|cccc} -181.50 & -81.78 & -22.19 & -3.79 & -2.07 & 0 & 0 & 0 & 0 \\ 128 & 0 & 0 & 0 & 0 & -200 & 0 & 0 & 0 \\ 0 & 32 & 0 & 0 & 0 & 0 & 0 & 0 & 0 \\ 0 & 0 & 4 & 0 & 0 & 0 & 0 & 0 & 0 \\ 0 & 0 & 0 & 4 & 0 & 0 & 0 & 0 & 0 \\ \hline 0 & 20000 & 0 & 0 & 0 & -4000 & 0 & -20000 & 0 \\ 0 & 0 & 0 & 0 & 0 & 0 & -1000 & -1123 & -457.8 \\ 0 & 0 & 0 & 0 & 0 & 1000 & 1024 & 0 & 0 \\ 0 & 0 & 0 & 0 & 0 & 0 & 0 & 256 & 0 \end{array}\right] \\ \underbrace{}_{\text{MG4}} \end{array} \tag{16}$$

Using (16), the eigenvalues for DCMG cluster in scenario 1 with actual gain and optimized gain values of the controller are shown in Fig. 18. It can be observed that the eigenvalues of the cluster after interconnection migrate to the right side of the *s*-plane, indicating an unstable state even though MG2 and MG4 are stable independently. Therefore, it can be inferred that the presence of a distribution line has affected the interconnected system stability. Hence, the controller gains need to be modified in order to bring the interconnected system to its stable mode of operation.

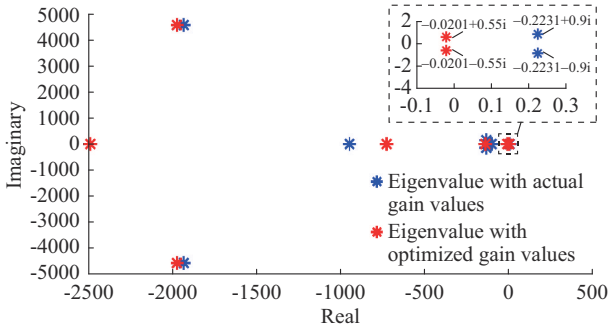

Fig. 18. Eigenvalues for DCMG cluster in scenario 1 with actual gain and optimized gain values of controller.

PSO is one of the most popular algorithms used for optimal tuning the controller gains [37], [38]. The objective function used for optimization is given in (17).

$$J = real(\lambda_i) < 0 \quad i = 1, 2, \ldots, n \tag{17}$$

s.t.

$$K_j^{\min} \le K_j \le K_j^{\max} \tag{18}$$

where $real(\lambda_i)$ is the real part of the i^{th} eigenvalue; n is the number of eigenvalues in the system; $K_j^{\min}$ is the minimum value of the j^{th} controller gain; and $K_j^{\max}$ is the maximum value of the j^{th} controller gain.

The algorithm is implemented in MATLAB and the parameters used in the optimization algorithm are as follows: population size is 100; acceleration constants $C_1 = C_2 = 2$; the maximum iteration is 20; the maximum inertia weight $w_{\max} = 0.9$; and the minimum inertia weight $w_{\min} = 0.4$.

The controller gains for case 1 are given in Table IV. The system matrix is given in (19) and the corresponding eigenvalue plot is given in Fig. 18. From Fig. 18, it can be ob-

served that the eigenvalues of the tuned DCMG cluster are on the left half of the *s*-plane and thus the system will operate in a stable mode.

TABLE IV
CONTROLLER GAINS FOR CASE 1

Controller parameter	Initial value	Optimal value
K_5	0.10	0.3494
K	0.55	1.2669
K	0.10	0.4823
K_8	0.10	0.1004
K_{13}	0.01	0.0299
K_{14}	8.00	0.6696

$$\overbrace{\begin{bmatrix} -818.6 & -284.2 & -43.39 & -3.814 & -2.396 & 0 & 0 & 0 & 0 \\ 256 & 0 & 0 & 0 & 0 & -200 & 0 & 0 & 0 \\ 0 & 64 & 0 & 0 & 0 & 0 & 0 & 0 & 0 \\ 0 & 0 & 4 & 0 & 0 & 0 & 0 & 0 & 0 \\ 0 & 0 & 0 & 2 & 0 & 0 & 0 & 0 & 0 \\ 0 & 20000 & 0 & 0 & 0 & -4000 & 0 & -20000 & 0 \\ 0 & 0 & 0 & 0 & 0 & 0 & -2492 & -877.7 & -76.63 \\ 0 & 0 & 0 & 0 & 0 & 1000 & 1024 & 0 & 0 \\ 0 & 0 & 0 & 0 & 0 & 0 & 0 & 128 & 0 \end{bmatrix}}^{\text{MG1}} \quad \overbrace{\phantom{\begin{bmatrix} 0 \\ 0 \\ 0 \\ 0 \\ 0 \\ 0 \\ 0 \\ 0 \\ 0 \end{bmatrix}}}^{\text{MG4}} \tag{19}$$

B. Scenario 2: Adding a DCMG Between Two Buses in a Distribution Line

In scenario 2, the cluster is formed by integrating MG3 in the middle of the distribution line connecting two DCMGs in a cluster, as shown in Fig. 19.

The system matrix of the interconnected system is given in (20) and the eigenvalues for DCMG cluster in scenario 2 with actual and optimized gain values of the controller is given in Fig. 20.

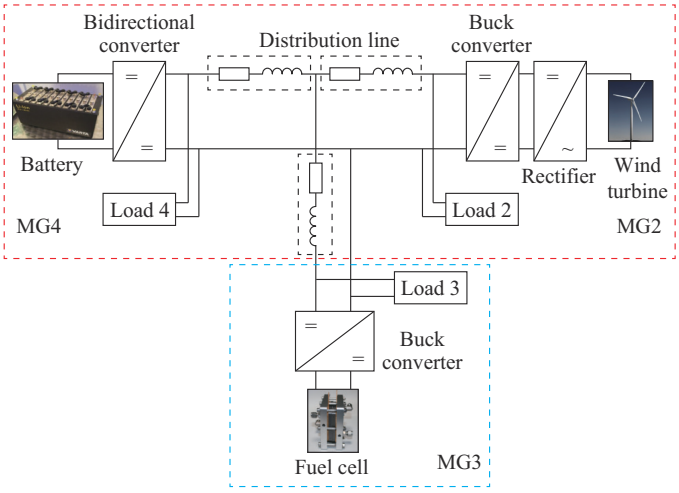

Fig. 19. DCMG cluster interconnecting a new DCMG in between a distribution line in existing cluster.

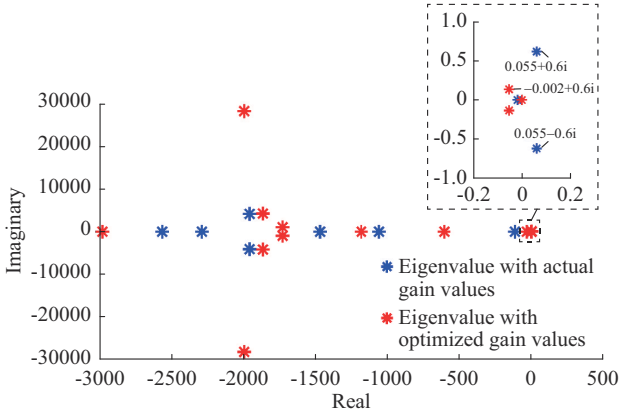

Fig. 20. Eigenvalues for DCMG cluster in scenario 2 with actual and optimized gain values of controller.

It can be observed that the system is unstable as it has eigenvalues on the right half of *s*-plane.

$$\overbrace{\begin{bmatrix} -818.65 & -284.2 & -43.39 & -3.81 & -2.39 & 0 & 0 & 0 & 0 & 0 & 0 & 0 & 0 & 0 \\ 256 & 0 & 0 & 0 & 0 & -200 & 0 & 0 & 0 & 0 & 0 & 0 & 0 & 0 \\ 0 & 64 & 0 & 0 & 0 & 0 & 0 & 0 & 0 & 0 & 0 & 0 & 0 & 0 \\ 0 & 0 & 4 & 0 & 0 & 0 & 0 & 0 & 0 & 0 & 0 & 0 & 0 & 0 \\ 0 & 0 & 0 & 2 & 0 & 0 & 0 & 0 & 0 & 0 & 0 & 0 & 0 & 0 \\ 0 & 20000 & 0 & 0 & 0 & -4000 & 0 & 0 & 0 & 0 & 0 & 0 & 0 & 0 \\ 0 & 0 & 0 & 0 & 0 & 0 & -2492 & -877.77 & -76.63 & 0 & 0 & 0 & 0 & 0 \\ 0 & 0 & 0 & 0 & 0 & 0 & 1024 & 0 & 0 & 1000 & 0 & 0 & 0 & 0 \\ 0 & 0 & 0 & 0 & 0 & 0 & 0 & 128 & 0 & 0 & 0 & 0 & 0 & 0 \\ 0 & 0 & 0 & 0 & 0 & 0 & 0 & -20000 & 0 & -4000 & 0 & 0 & 0 & 0 \\ 0 & 0 & 0 & 0 & 0 & 0 & 0 & 0 & 0 & 0 & -4000 & 0 & 20000 & 0 \\ 0 & 0 & 0 & 0 & 0 & 0 & 0 & 0 & 0 & 0 & 0 & -115.20 & -137.80 & -59.19 \\ 0 & 0 & 0 & 0 & 0 & 0 & 0 & 0 & 0 & 0 & -40000 & 256 & 0 & 0 \\ 0 & 0 & 0 & 0 & 0 & 0 & 0 & 0 & 0 & 0 & 0 & 0 & 32 & 0 \end{bmatrix}}^{\text{MG1}} \quad \overbrace{\phantom{\begin{bmatrix} 0 \\ 0 \\ 0 \\ 0 \\ 0 \\ 0 \\ 0 \\ 0 \\ 0 \\ 0 \\ 0 \\ 0 \\ 0 \\ 0 \end{bmatrix}}}^{\text{MG3}} \tag{20}$$

The controller gains for scenario 2 are shown in Table V. It can be inferred from Fig. 20 that the system is now stable as all eigenvalues are on the left half of the *s*-plane.

TABLE V
CONTROLLER GAINS FOR SCENARIO 2

Controller parameter	Initial value	Optimum value
K_5	0.3494	0.9716
K_6	1.2669	1.7434
K_7	0.4823	1.4560
K_8	0.1004	0.0207
K_9	0.0100	0.0641
K_{10}	2.0000	1.3629
K_{13}	0.0299	0.0094
K_{14}	0.6696	1.2990

C. Scenario 3: Adding a New DCMG at One End of a Distribution Line in DCMG Cluster

The cluster in scenario 3 is obtained by interconnecting MG1 at one end of a distribution line in a DCMG cluster, as shown in Fig. 21.

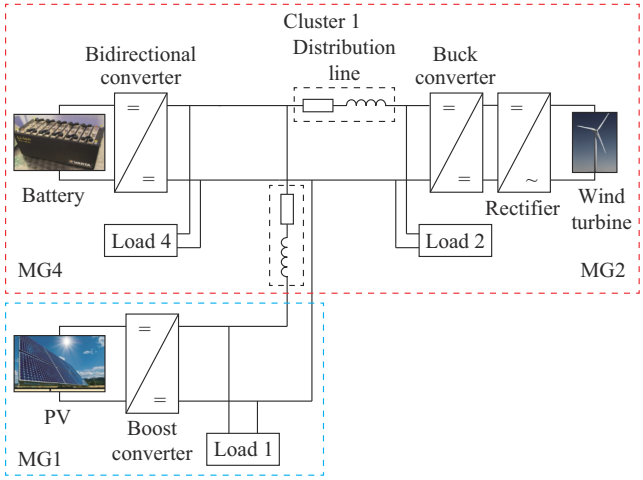

Fig. 21. DCMG cluster interconnecting a new DCMG at one end of distribution line.

The system matrix of the DCMG cluster after interconnection is obtained as (21). The eigenvalue plot of the system is presented in Fig. 22. As in previous cases, here also, the system is unstable due to the presence of eigenvalues in the right half of *s*-plane. The controller gains for scenario 3 are given in Table VI.

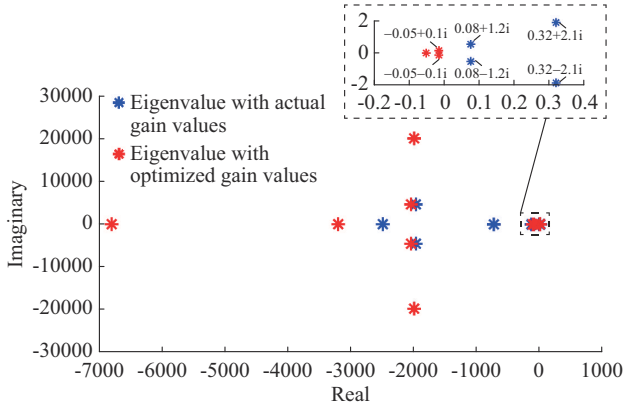

Fig. 22. Eigenvalues for DCMG cluster in scenario 3 with actual and optimized gain values of controller.

TABLE VI
CONTROLLER GAINS FOR SCENARIO 3

Controller parameter	Initial value	Optimal value	Controller parameter	Initial value	Optimal value
K_1	0.0900	0.0298	K_6	1.2669	0.2033
K_2	1.0000	0.0927	K_7	0.4823	1.1945
K_3	0.1000	0.1516	K_8	0.1004	0.0664
K_4	5.0000	7.6143	K_{13}	0.0299	0.0892
K_5	0.3494	0.2736	K_{14}	0.6696	0.1241

Figure 22 shows that the system became stable after tuning the controller gains.

The stability of a DCMG cluster during interconnection, considering the impact of the distribution line, is examined in this investigation. Additionally, it is demonstrated how beneficial is the controller gain adjustment in maintaining the stability of DCMG cluster.

MG1

$$\begin{bmatrix}
-818.65 & -284.2 & -43.39 & -3.814 & -2.396 & 0 & 0 & 0 & 0 & 0 & 0 & 0 & 0 & 0 & 0 \\
256 & 0 & 0 & 0 & 0 & -200 & 0 & 0 & 0 & 200 & 0 & 0 & 0 & 0 & 0 \\
0 & 64 & 0 & 0 & 0 & 0 & 0 & 0 & 0 & 0 & 0 & 0 & 0 & 0 & 0 \\
0 & 0 & 4 & 0 & 0 & 0 & 0 & 0 & 0 & 0 & 0 & 0 & 0 & 0 & 0 \\
0 & 0 & 0 & 2 & 0 & 0 & 0 & 0 & 0 & 0 & 0 & 0 & 0 & 0 & 0 \\
0 & 20000 & 0 & 0 & 0 & -4000 & 0 & -20000 & 0 & 0 & 0 & 0 & 0 & 0 & 0 \\
0 & 0 & 0 & 0 & 0 & 0 & -2492 & -877.77 & -76.63 & 0 & 0 & 0 & 0 & 0 & 0 \\
0 & 0 & 0 & 0 & 0 & 1000 & 1024 & 0 & 0 & 0 & 0 & 0 & 0 & 0 & 0 \\
0 & 0 & 0 & 0 & 0 & 0 & 0 & 128 & 0 & 0 & 0 & 0 & 0 & 0 & 0 \\
0 & -20000 & 0 & 0 & 0 & 0 & 0 & 0 & 0 & -4000 & 0 & 20000 & 0 & 0 & 0 \\
0 & 0 & 0 & 0 & 0 & 0 & 0 & 0 & 0 & 0 & -91.8 & -105.1 & -62.53 & -25.05 & -14.13 \\
0 & 0 & 0 & 0 & 0 & 0 & 0 & 0 & 0 & -20000 & 128 & 0 & 0 & 0 & 0 \\
0 & 0 & 0 & 0 & 0 & 0 & 0 & 0 & 0 & 0 & 0 & 64 & 0 & 0 & 0 \\
0 & 0 & 0 & 0 & 0 & 0 & 0 & 0 & 0 & 0 & 0 & 0 & 32 & 0 & 0 \\
0 & 0 & 0 & 0 & 0 & 0 & 0 & 0 & 0 & 0 & 0 & 0 & 0 & 8 & 0
\end{bmatrix} \quad (21)$$

MG3

D. Variation of Eigenvalues with Different Controller Gains

Every time, tuning the controller gains brings the unstable cluster to the stable operation mode. It implies that the system eigenvalues move from the right half of *s*-plane to the left during optimization. Figure 23 shows the variation of eigenvalues for different controller gains. It can be observed that the eigenvalues of the interconnected system move from the right half of *s*-plane to the left half of *s*-plane, making the interconnected system stable.

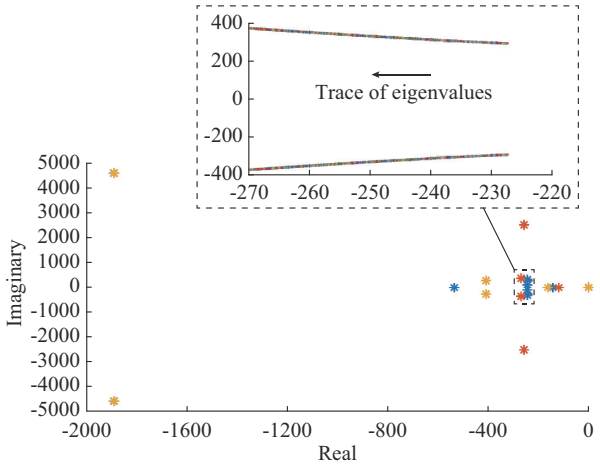

Fig. 23. Variation of eigenvalues for different controller gains.

VI. Simulation Results

The step response of the system is assessed to verify the proposed SMB algorithm. To determine the system stability, the step response of the individual DCMGs is first assessed separately. The step response for the cluster is then assessed after the stable DCMGs are interconnected through a distribution line.

The step response of the two independent DCMGs (MG2 and MG4) is given in Section III, and the response indicates that the individual DCMGs are stable and are shown in Fig. 24.

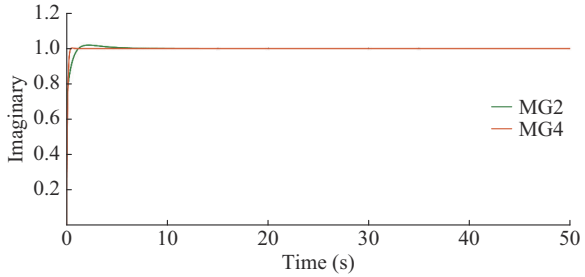

Fig. 24. Step response of individual DCMGs (MG2 and MG4).

The DCMG cluster is formed by interconnecting MG2 and MG4, which are stable while operating independently. The general block diagram representation of the DCMG cluster with the MGs interconnected using a distribution line is is given in Fig. 25.

The block diagram includes a transfer function model for both MGs and a distribution line connecting the two systems. The step response of the cluster with initial gain values is shown in Fig. 26. It can be observed that the response deviates significantly and the cluster becomes unstable due to the presence of a distribution line in the cluster. PSO algorithm is employed to fine-tune the controller gains in order to stabilize the system. As a result, as illustrated in Fig. 27, the unstable cluster is stabilized with the modified optimal gains and the response settles without any steady state error. The results obtained during the simulation studies are validated using real-time analysis.

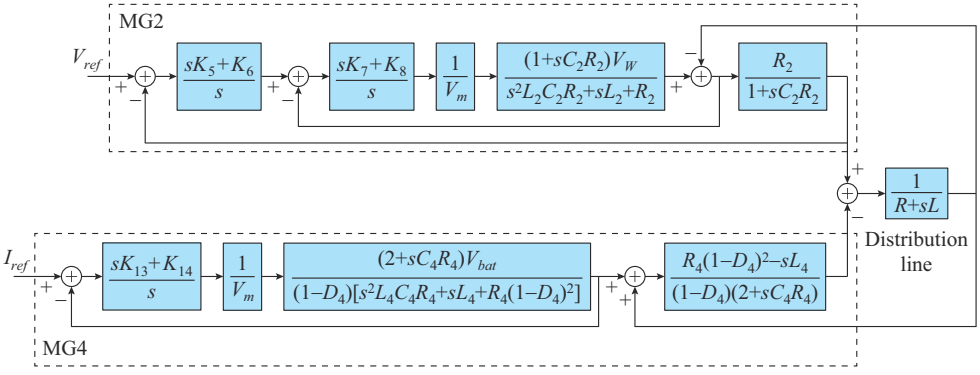

Fig. 25. Block diagram representation of DCMG cluster with MGs interconnected using a distribution line.

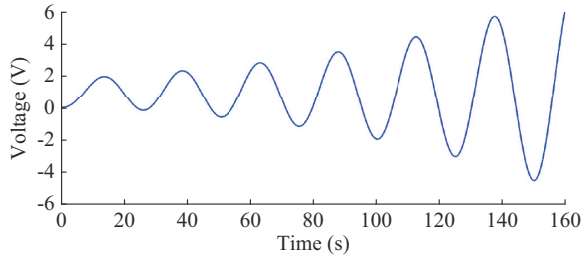

Fig. 26. Step response of cluster with initial gain values.

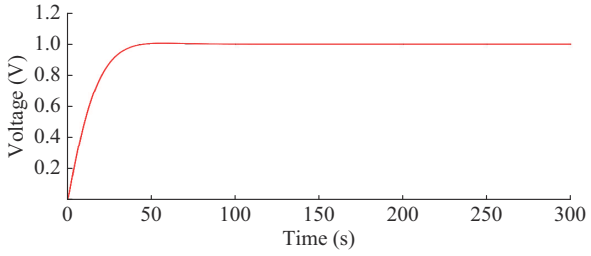

Fig. 27. Step response of cluster with optimal gain values.

VII. Experimental Study: Real-time Analysis

The experimental set-up using OP4510 real-time simulator is used to experimentally validate the proposed SMB algorithm in real time and is shown in Fig. 28. For the validation, the DCMG cluster of case 1 shown in Fig. 25 is considered. The system parameters used in the paper are listed in Table IV.

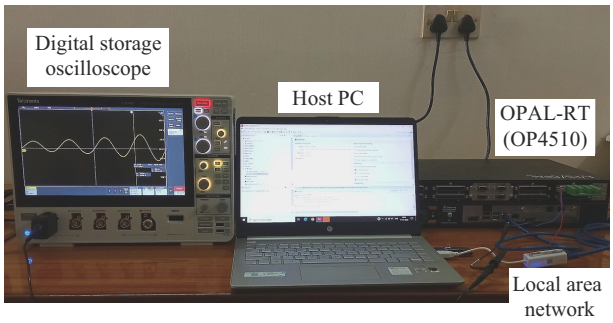

Fig. 28. Experimental setup for real-time analysis.

The step response of the individual DCMGs with the initial gain values is shown in Fig. 29 and it can be observed that both the MGs are operating stably. The response of the DCMG cluster after being interconnected through a distribution line is shown in Fig. 30. It is evident that the resulting DCMG cluster is unstable. The best method for stabilizing the resulting DCMG cluster is to re-tune the controller gains in the new cluster. The response of the DCMG cluster with the controller gains tuned using PSO is shown in Fig. 31. It is clear that the response of the DGMG cluster with optimally tuned controller gains is stable. These outcomes vouch for the viability of the proposed SMB algorithm for stability analysis of DCMG cluster.

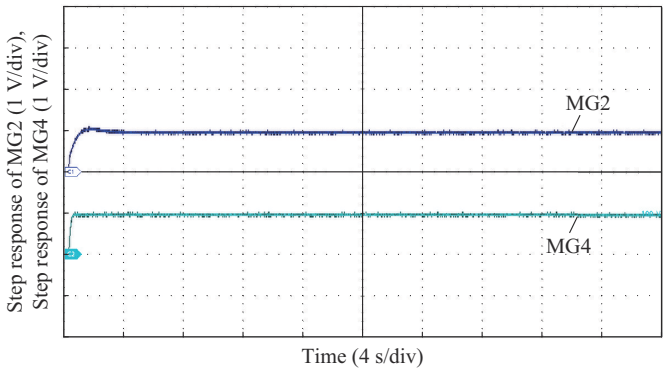

Fig. 29. Step response of individual DCMGs (MG2 and MG4) with initial gain values.

VIII. Conclusion

In this paper, modeling and stability problems in DCMG clusters are examined. Three possible cases are considered in this paper: ① adding a new network to an existing network, ② adding a new network in between a distribution line, and ③ adding a new network at one end of a distribution line in a cluster. A step-by-step programmable technique has been developed to update the system matrix of the DCMG cluster after interconnection.

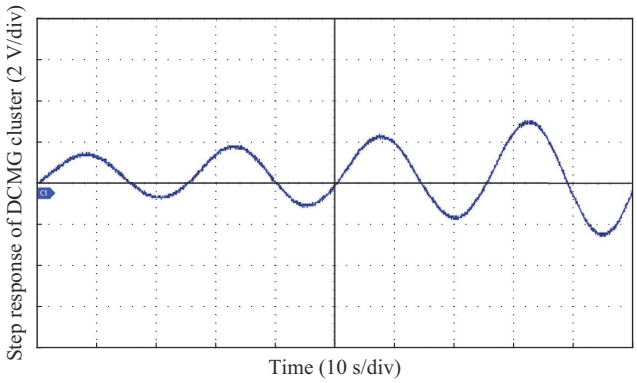

Fig. 30. Step response of DCMG cluster with initial gain values.

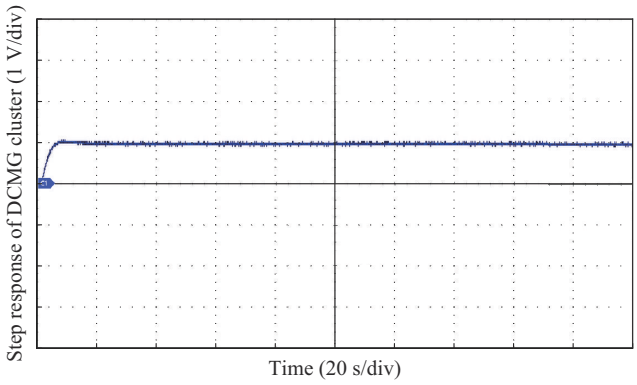

Fig. 31. Step response of DCMG cluster with controller gains tuned using PSO.

With the developed method, adding a new network to an existing network has the benefit of not necessitating a total rebuilding of the system matrix.

Even though the extant DCMG network and the incoming DCMG are both stable, it has been found that, while interconnecting through a distribution line, the system stability is affected. To stabilize the new cluster, PSO is applied to modify the controller gains. The response of the interconnected DCMG with optimally tuned controller gains indicates that stable operation is ensured. In addition, the novel step-by-step SMB algorithm can be adapted to build the system matrix of the interconnected system to perform the stability analysis. The simulation and real-time results prove the significance of the proposed SMB algorithm.

References

[1] L. Xu, J. M. Guerrero, A. Lashab *et al*., "A review of DC shipboard microgrids part II: control architectures, stability analysis, and protection schemes," *IEEE Transactions on Power Electronics*, vol. 37, no. 4, pp. 4105-4120, Apr. 2022.

[2] P. Silva and C. Medeiros, "A promising future to DC power system: a review," *IEEE Latin America Transactions*, vol. 15, no. 9, pp. 1639-1642, Sept. 2017.

[3] Z. Sun and S. Bae, "Multiple-input soft-switching DCDC converter to connect renewable energy sources in a DC microgrid," *IEEE Access*, vol. 10, pp. 128380-128391, Feb. 2022.

[4] Y. Gui, R. Han, J. M. Guerrero *et al*., "Large-signal stability improvement of DC-DC converters in DC micro-grid," *IEEE Transactions on Energy Conversion*, vol. 36, no. 3, pp. 2534-2544, Sept. 2021.

[5] S. Ferahtia, A. Djerioui, H. Rezk *et al*., "Adaptive droop based control strategy for dc microgrid including multiple batteries energy storage systems," *Journal of Energy Storage*, vol. 48, p. 103983, Feb. 2022.

[6] K. Jithin, N. Mayadevi, R. H. Kumar *et al*., "The effect of multiple PV and battery penetration on stability of dc microgrid with single bus topology," in *Proceedings of 2021 9th IEEE International Conference on Power Systems (ICPS)*, Bhubaneswar, India, Dec. 2021, pp. 1-5.
[7] K. Jithin, P. P. Haridev, N. Mayadevi *et al*., "A review on challenges in DC microgrid planning and implementation," *Journal of Modern Power Systems and Clean Energy*, vol. 11, no. 5, pp. 1375-1395, Sept. 2023.
[8] H. Yu, S. Niu, Z. Shao *et al*., "A scalable and reconfigurable hybrid AC/DC microgrid clustering architecture with decentralized control for coordinated operation," *International Journal of Electrical Power & Energy Systems*, vol. 135, p. 107476, Feb. 2022.
[9] M. Zaery, P. Wang, W. Wang *et al*., "A novel optimal power allocation control system with high convergence rate for DC microgrids cluster," *Energies*, vol. 15, p. 107476, May 2022.
[10] M. Leng, G. Zhou, G. Xu *et al*., "Small-signal stability assessment and interaction analysis for bipolar DC microgrids," *IEEE Transactions on Power Electronics*, vol. 34, no. 4, pp. 5524-5537, Apr. 2023.
[11] L. Yang, Q. Zhang, S. Liu *et al*., "Impedance-based small-signal stability analysis of DC microgrid clusters," in *Proceedings of 2022 IEEE International Power Electronics and Application Conference and Exposition (PEAC)*, Guangzhou, China, Nov. 2022, pp. 1579-1584.
[12] A. A. Derbas, A. Oshnoei, M. Azzouz *et al*., "Adaptive damping control to enhance small-signal stability of DC microgrids," *IEEE Journal of Emerging and Selected Topics in Power Electronics*, vol. 11, no. 3, pp. 2963-2978, Jun. 2023.
[13] L. Wang, X. Peng, H. Yang *et al*., "Stability analysis of a grid-connected large-scale DC microgrid with a hybrid wind/solar farm," in *Proceedings of 2022 IET International Conference on Engineering Technologies and Applications (IET-ICETA)*, Taiwan, China, Oct. 2022, pp. 1-2.
[14] M. Leng, G. Zhou, H. Li *et al*., "Impedance-based stability evaluation for multibus DC microgrid without constraints on subsystems," *IEEE Transactions on Power Electronics*, vol. 37, no. 1, pp. 932-943, Jun. 2021.
[15] A. Aluko, A. Swanson, L. Jarvis *et al*., "Modeling and stability analysis of distributed secondary control scheme for standalone DC microgrid applications," *Energies*, vol. 15, no. 15, p. 5411, Jul. 2022.
[16] A. C. Braitor, "Admittance matrix computation and stability analysis of droop-controlled DC microgrids," in *Advanced Hierarchical Control and Stability Analysis of DC Microgrids*. Cham: Springer, 2022, pp. 55-65.
[17] S. Kotra and M. K. Mishra, "Design and stability analysis of DC microgrid with hybrid energy storage system," *IEEE Transactions on Sustainable Energy*, vol. 10, no. 3, pp. 1603-1612, Jul. 2019.
[18] W. Xie, M. Han, W. Cao *et al*., "System-level large-signal stability analysis of droop-controlled DC microgrids," *IEEE Transactions on Power Electronics*, vol. 36, no. 4, pp. 4224-4236, Apr. 2021.
[19] S. Liu, X. Li, M. Xia *et al*., "Takagi-Sugeno multimodeling-based large signal stability analysis of DC microgrid clusters," *IEEE Transactions on Power Electronics*, vol. 36, no. 11, pp. 12670-12684, Nov. 2021.
[20] A. El-Shahat and S. Sumaiya, "DC-microgrid system design, control, and analysis," *Electronics*, vol. 8, no. 2, p. 124, Jan. 2019.
[21] Z. Li, W. Pei, H. Ye *et al*., "Large signal stability analysis for DC microgrid under droop control based on mixed potential theory," *The Journal of Engineering*, vol. 2019, no. 16, pp. 1189-1193, Mar. 2019.
[22] M. Naderi, Y. Khayat, Q. Shafiee *et al*., "Dynamic modeling, stability analysis and control of interconnected microgrids: a review," *Applied Energy*, vol. 334, p. 120647, Mar. 2023.
[23] Z. Liu, J. Zhao, K. Qu *et al*., "A small-signal stability criterion for DC microgrid based on extended-gershgorin theorem," *IEEE Transactions on Power Delivery*, vol. 38, no. 3, pp. 2047-2057, Jun. 2023.
[24] M. Dong, L. Li, Y. Nie *et al*., "Stability analysis of a novel distributed secondary control considering communication delay in DC microgrids," *IEEE Transactions on Smart Grid*, vol. 10, no. 6, pp. 6690-6700, Nov. 2019.
[25] F. Perez, A. Iovine, G. Damm *et al*., "Stability analysis of a DC microgrid for a smart railway station integrating renewable sources," *IEEE Transactions on Control Systems Technology*, vol. 28, no. 5, pp. 1802-1816, Sept. 2020.
[26] A. M. Mustafa, M. E. Nassar, M. Salama *et al*., "Voltage-sag mitigation by stability-constrained partitioning scheme," *Ain Shams Engineering Journal*, vol. 14, no. 2, pp. 10-18, Mar. 2023.
[27] M. Pourmohammad, M. Toulabi, M. Rayati *et al*., "Load type impacts on the stability and robustness of DC microgrids," *International Journal of Electrical Power & Energy Systems*, vol. 140, p. 108036, Sept. 2022.
[28] W. E. Robert and D. Maksimovie, *Fundamentals of Power Electronics*. New York: Springer, 2004, pp. 265-482.
[29] K. Jithin, R. Harikumar, N. Mayadevi *et al*., "A centralized control algorithm for power management in interconnected DC microgrids," in *Proceedings of Symposium on Power Electronic and Renewable Energy Systems Control*, Kharaghpur, India, Jun. 2021, pp. 451-461.
[30] A. Kaysal, S. Koroglu, Y. Oguz *et al*., "Design and experimental implementation of DC-DC converter based self-tuning fuzzy PI controller," *Journal of the Faculty of Engineering and Architecture of Gazi University*, vol. 38, no. 1, pp. 483-495, Jun. 2023.
[31] A. S. Samosir, T. Sutikno, and L. Mardiyah, "Simple formula for designing the PID controller of a DC-DC buck converter," *International Journal of Power Electronics and Drive Systems*, vol. 14, no. 1, p. 327, Mar. 2023.
[32] J. Teh, C. Lai, and Y. Cheng, "Impact of the real-time thermal loading on the bulk electric system reliability," *IEEE Transactions on Reliability*, vol. 66, no. 4, pp. 1110-1119, Dec. 2017.
[33] C. Lai and J. Teh, "Comprehensive review of the dynamic thermal rating system for sustainable electrical power systems," *Energy Reports*, vol. 8, pp. 3263-3288, Nov. 2022.
[34] L. Ge, Y. Li, J. Yan *et al*., "Smart distribution network situation awareness for high-quality operation and maintenance: a brief review," *Energies*, vol. 15, p. 828, Jan. 2022.
[35] C. Guo, C. Ye, Y. Ding *et al*., "A multi-state model for transmission system resilience enhancement against short-circuit faults caused by extreme weather events," *IEEE Transactions on Power Delivery*, vol. 36, no. 4, pp. 2374-2385, Aug. 2021.
[36] Y. Wang, X. Wen, B. Gu *et al*., "Power scheduling optimization method of wind-hydrogen integrated energy system based on the improved AUKF algorithm," *Mathematics*, vol. 10, p. 4207, Nov. 2022.
[37] Z. Fan, W. Zhang, and W. Liu, "Multi-agent deep reinforcement learning based distributed optimal generation control of DC microgrids," *IEEE Transactions on Smart Grid*, vol. 14, no. 5, pp. 3337-3351, Sept. 2023.
[38] A. A. El-Ela, H. A. Mosalam, and R. A. Amer, "Optimal control design and management of complete dc-renewable energy microgrid system," *Ain Shams Engineering Journal*, vol. 14, no. 5, p. 101964, Sept. 2023.

K. Jithin received the B.Tech. degree in electrical and electronics engineering and the M.Tech. degree in power systems from College of Engineering Trivandrum, Thiruvananthapuram, India, under APJ Abdul Kalam Technological University (APJAKTU), Trivandrum, India, in 2015 and 2018, respectively. He is currently a Research Scholar at APJAKTU. His research interests include DC microgrid, renewable power generation, and interconnected DC microgrids.

N. Mayadevi received the B.Tech in electrical and electronics engineering from Rajiv Gandhi Institute of Technology Kottayam, Kottayam, India, the M.Tech degree in computer and information sciences from Cochin University of Science and Technology, Ernakulam, India, and the Ph.D. degree from the University of Kerala, Ernakulam, India. She is currently working as a Professor at the Department of Electrical Engineering, College of Engineering Trivandrum, Trivandrum, India. Her research interests include machine learning, supervisory control and data acquisition (SCADA), and database systems.

R. Hari Kumar received the B.E. degree in electrical and electronics engineering from the Manipal Institute of Technology, Manipal, India, in 1995, the M.Tech. degree in power systems from the National Institute of Engineering, Mysore, India, in 2006, and the Ph.D. degree in electrical engineering from Kerala University, Trivandrum, India, in 2018. Since 2008, he has been with the Department of Electrical Engineering, College of Engineering Trivandrum, Trivandrum, India, where he is currently working as an Associate Professor. His current research interests include the control and protection of microgrids, smart grids, and electric drives.

V. P. Mini received the B.Tech. degree in electrical and electronics engineering from MA College of Engineering, Kottayam, India, in 1991, the M.Tech. degree from National Institute of Technology Trichy, Trichy, India, in 2006, and the Ph. D. degree from University of Kerala, Trivandrum, India, in 2015. She is currently working as Professor at the Department of Electrical Engineering, College of Engineering Trivandrum, Trivandrum, India. Her research interests include electric vehicles, electric drives, and fuzzy logic.